Available online at www.sciencedirect.com

SCIENCE DIRECT®

PERGAMON

International Journal of Multiphase Flow 29 (2003) 751–769

International Journal of Multiphase Flow

www.elsevier.com/locate/ijmulflow

Simulation of the sedimentation of melting solid particles

Hui Gan [a], James J. Feng [a,*], Howard H. Hu [b]

[a] *The Levich Institute for Physicochemical Hydrodynamics, City College of the City University of New York, New York, NY 10031, USA*

[b] *Department of Mechanical Engineering and Applied Mechanics, University of Pennsylvania, Philadelphia, PA 19104, USA*

Received 23 October 2002; received in revised form 11 February 2003

Abstract

This study is motivated by the fact that dispersed two-phase flows are often accompanied by interfacial activities such as chemical reaction and phase change. Toward an understanding of the role of interfacial transport, we numerically simulate the sedimentation of melting solid particles in a Newtonian fluid. The fluid flow and solid motion determine the fluid–solid heat transfer and hence the melting rate. The thermal convection and interfacial morphology, in return, affect the motion of both phases. The two-dimensional Navier–Stokes and energy equations are solved at moderate Reynolds numbers by a finite-element method, and the melting interface is determined from the local heat flux. The motion of each solid particle is tracked using an arbitrary Lagrangian–Eulerian scheme. Results show that the sedimentation of melting particles is largely governed by the competition between the upward flow of the warm upstream fluid and the downward flow of the cold melt. A single particle settling in a channel may be pushed away from the centerline toward the wall. A pair of particles interact in a complex way, separating at low Grashof number *Gr* and attracting each other at high *Gr*. These results have interesting implications for the formation of microstructures in interfacially active two-phase flows.

Keywords: Numerical simulation; Two-phase flow; Phase change; Suspension microstructure

1. Introduction

Multiphase flows in industry often involve interfacial activities such as phase change and chemical reactions. A quintessential example is the fluidized bed reactor. Not only do the particles

* Corresponding author.
E-mail address: feng@ccny.cuny.edu (J.J. Feng).

0301-9322/03/$ - see front matter
doi:10.1016/S0301-9322(03)00035-1

and fluid exchange momentum across moving interfaces, but the chemical reactions also introduce heat and mass transfer (HMT) into the problem and erode the solid surfaces. The coupling among various processes imparts a complexity to the system far beyond that of inert multiphase flows.

It is then not surprising that our current knowledge of interfacially active two-phase flows is limited. Previous work has mostly been done in the context of spray combustion, and can be put roughly into two categories. The first category includes detailed investigations of the flow, temperature and composition fields near one or a few fuel drops. For instance, Ayyaswamy (1999) solved the transport equations for momentum, energy and species in and outside of a burning drop. Chiang and Sirignano (1993) studied the vaporization of two drops moving in tandem in a hot gas stream, and numerically predicted the drag coefficient, Nusselt number and Sherwood number. Thermal and compositional convections were neglected in these studies, and the drops remain spherical because of surface tension. Compositional convection and changing surface morphology are the focus of several experiments on the melting or dissolution of solid particles in a sea of hot fluids (Kerr, 1994; McLeod et al., 1996). Interesting morphology develops on the solid surface, and is intimately coupled with the flow field and HMT. McLeod et al. (1996) used scaling arguments to predict the speed of melting based on the Rayleigh–Taylor instability of the melt layer. No rigorous theory or numerical simulations have been attempted.

The second category contains studies of many moving particles with phase change or reaction on their surface. First-principle solutions based on rigorous governing equations are no longer possible, and detailed physics at the interface has to be sacrificed in favor of phenomenology. Two types of models have been developed: the effective-continuum model and the trajectory model (Crowe, 1991; Sirignano, 1993). The former treats the droplets as an effective continuum and is in essence a generalized two-fluid model (Ishii, 1975). The latter recognizes the necessity of tracking discrete droplets, and achieves this by using correlations, say, for the drag and lift coefficients (Delnoij et al., 1997). In both models, the mass, momentum and heat transfer between the gas and the droplets must be provided as inputs; these may come from experimental data, phenomenological calculations using, say, the cell model (Bellan, 1991), or accurate calculations for a single droplet (Sirignano, 1999).

Indeed, there are applications where it is impossible or unnecessary to account for the mesoscopic features, and a continuum model suffices. In general, however, heat and mass transfer and reaction rate are strong functions of the phase morphology, which, in turn, is dictated by the motion and interaction of individual particles (Joseph, 1996). Toward the goal of direct numerical simulation of particulate flows, several groups developed computational methods to track individual particles (see Hu et al., 2001 for a review). Recently, such methods have been applied to HMT and phase change near moving particles and deforming interfaces. Juric and Tryggvason (1998) and Shin and Juric (2002) simulated film boiling on a heated plate. By tracking the position of the water-vapor interface, they were able to reproduce the detachment of vapor bubbles and the complex topological changes in the process. Hao and Prosperetti (2000) studied the motion of a vapor bubble in a nonuniform channel. The flow outside is taken to be a potential flow, and the pressure and the slip on the bubble's surface determine the condensation of the vapor. Gan et al. (2003) demonstrated how thermal convection modifies the motion and interaction of sedimenting particles. Particles colder than the fluid tend to disperse while hotter particles tend to aggregate. The drafting-kissing-tumbling scenario well documented for isothermal sedimentation is all but inhibited.

This paper extends our previous effort by introducing phase change. We report two-dimensional simulations of the motion and interaction of particles settling and melting in a hot fluid. The two phases are of the same material so the melting involves heat transfer but not mass transfer. This problem seems to be the simplest to contain the essentials of interfacially active multiphase flows. Generalization to other forms of phase transition such as solidification, vaporization and condensation is straightforward. By adding a convection-diffusion equation for species, the method can also be applied to two-phase flows with dissolution/precipitation or rapid, irreversible heterogeneous surface reactions.

The rest of the paper is organized as follows. Section 2 formulates the problem and discusses the theoretical model and numerical methods. Section 3 describes validation of the numerical scheme using test problems. Sections 4 and 5 discuss, respectively, the sedimentation of a single particle and the interaction between two particles. Conclusions are drawn in Section 6.

2. Problem formulation

We release solid particles with zero initial velocity in a vertical channel filled with a Newtonian fluid (Fig. 1). In two dimensions, the particles are circles. The solid is at its melting temperature T_m and the fluid has a uniform initial temperature $T_0 > T_m$. The particles start to melt while settling under gravity. We assume that the two phases are made of the same material so we need not consider mass transfer or compositional convection. Setting the initial solid temperature at T_m may seem artificial. But it does not seriously compromise the objective of this study since subcooling would affect only the initial transient. In general, we must note, transient heating of the particles can be an appreciable effect if the solid thermal diffusivity is not very large (Sirignano, 1999). Because of the macroscopic size of the particles, the Gibbs–Thomson effect on T_m is negligible (Jackson and McKenna, 1990). Admittedly, a particle settling in its own melt is a special case with limited practical significance. However, our rationale is to use this simplified problem to elucidate the basic physical mechanisms, which are likely relevant to more general two-phase flows with phase transition and chemical reaction. By the same token, the parameters used in the simulations are not intended to represent a particular material or process. For instance, we have chosen the solid and fluid densities freely to access various settling regimes, with no regard to the fact that the density usually differs little between a solid and its melt.

The continuity, momentum and energy equations for the fluid are:

$$\nabla \cdot \boldsymbol{v} = 0, \tag{1}$$

$$\rho_0 \left(\frac{\partial \boldsymbol{v}}{\partial t} + \boldsymbol{v} \cdot \nabla \boldsymbol{v} \right) = -\nabla p + \mu \nabla^2 \boldsymbol{v} + \rho \boldsymbol{g}, \tag{2}$$

$$\rho_0 c_p \left(\frac{\partial T}{\partial t} + \boldsymbol{v} \cdot \nabla T \right) = k \nabla^2 T. \tag{3}$$

In Eq. (2), we use the Boussinesq approximation such that a temperature change only modifies the fluid density ρ in the body force term:

$$\rho = \rho_0 [1 - \beta (T - T_0)], \tag{4}$$

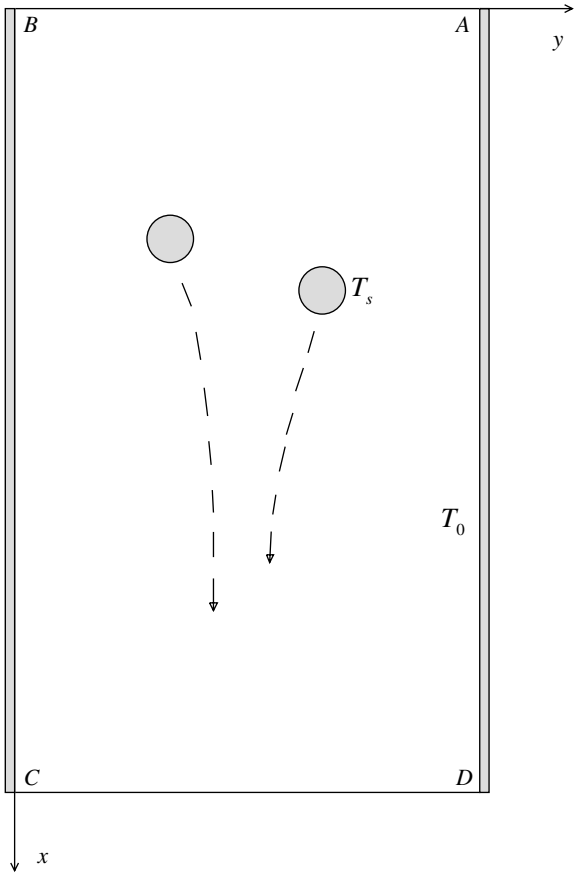

Fig. 1. Schematic of the computational domain. The initial fluid temperature is T_0 and the solid temperature is fixed at T_m.

where ρ_0 is the fluid density at the far-field temperature T_0, and β is the coefficient of thermal expansion for the fluid. In Eq. (3), we have neglected viscous dissipation since the Eckert number is typically small in our simulations (cf. White, 1991, p. 84). The ith particle translates and rotates according to the following equations:

$$m_i \frac{d\boldsymbol{V}_i}{dt} = \boldsymbol{G}_i + \boldsymbol{F}_i, \tag{5}$$

$$I_i \frac{d\boldsymbol{\Omega}_i}{dt} = \boldsymbol{T}_i, \tag{6}$$

where m_i and I_i are the instantaneous mass and moment of inertia of the particle, $\boldsymbol{V}_i$ and $\boldsymbol{\Omega}_i$ are its velocity and angular velocity, and $\boldsymbol{G}_i$, $\boldsymbol{F}_i$ and $\boldsymbol{T}_i$ are the body force, hydrodynamic force and moment, respectively.

The motion of the particles and the fluid flow are coupled via the hydrodynamic force and moment and boundary conditions on the particle surfaces. We impose continuity of velocity (no-

slip) and temperature on the particles. Since melting usually involves negligible volume change, we need not introduce a jump in the normal velocity at the particle surface as is necessary for vaporization (Ayyaswamy, 1999). The rate of melting is determined by the local heat flux on the particle surface, which recedes according to the following condition:

$$\rho_s h_f \frac{dr_n}{dt} = -k \frac{\partial T}{\partial n}, \tag{7}$$

where ρ_s is the solid density, h_f is the latent heat of fusion, and r_n is the coordinate of the particle surface along the local normal $\boldsymbol{n}$. Obviously, the particle changes shape as a result of nonuniform melting. On the four sides of the channel we impose the following conditions (see Fig. 1):

$$\boldsymbol{v} = \boldsymbol{0}, \quad T = T_0 \text{ on BC, CD and DA},$$
$$\tau_{xy} = \tau_{xx} = 0, \quad \partial T/\partial x = 0 \text{ on AB},$$

where τ represents total stress components. In our simulations, the computational domain is redefined at every time step such that its top and bottom are at prescribed distances from the particles. Therefore, with $\boldsymbol{v} = \boldsymbol{0}$ at *CD*, we simulate sedimentation in a channel so deep that the particles drive zero net flow rate.

The governing equations are non-dimensionalized by scaling length by the initial particle diameter d, velocity by an as yet unspecified U, and pressure, forces and torques by $\mu U/d$, μU and $\mu U d$, respectively. The dimensionless temperature is defined as $(T - T_m)/(T_0 - T_m) = (T - T_m)/\Delta T$. Using the same symbols for the dimensionless quantities, we re-write Eqs. (1)–(3), (5)–(7) as

$$\nabla \cdot \boldsymbol{v} = 0, \tag{8}$$

$$Re\left(\frac{\partial \boldsymbol{v}}{\partial t} + \boldsymbol{v} \cdot \nabla \boldsymbol{v}\right) = -\nabla p + \nabla^2 \boldsymbol{v} - \frac{Gr}{Re} T \hat{\boldsymbol{i}}, \tag{9}$$

$$\left(\frac{\partial T}{\partial t} + \boldsymbol{v} \cdot \nabla T\right) = \frac{1}{RePr} \nabla^2 T, \tag{10}$$

$$\frac{\pi}{4} \frac{\rho_s}{\rho_0} m_i Re \frac{d\boldsymbol{V}_i}{dt} = \boldsymbol{G}_i + \boldsymbol{F}_i, \tag{11}$$

$$\frac{\pi}{32} \frac{\rho_s}{\rho_0} I_i Re \frac{d\boldsymbol{\Omega}_i}{dt} = \boldsymbol{T}_i, \tag{12}$$

$$\frac{1}{St} \frac{dr_n}{dt} = -\frac{1}{RePr} \frac{\partial T}{\partial n}, \tag{13}$$

where $\hat{\boldsymbol{i}}$ is the unit vector along the x-axis, and m_i and I_i have been scaled by their initial values $\pi \rho_s d^2/4$ and $\pi \rho_s d^4/32$, respectively. The hydrostatic pressure has been absorbed into p, and $\boldsymbol{G}_i$ includes the buoyancy force due to $\rho_0 \boldsymbol{g}$. The dimensionless parameters are:

Reynolds number: $Re = \dfrac{\rho_0 U d}{\mu}$,

Grashof number: $Gr = \dfrac{\rho_0^2 \beta \Delta T d^3 g}{\mu^2}$,

Prandtl number: $Pr = \dfrac{\mu c_p}{k}$,

Stefan number: $St = \dfrac{c_p \Delta T}{h_f}$.

Note that the dimensionless temperature gradient $\partial T/\partial n$ in Eq. (13) is in fact the local Nusselt number (Nu) on the particle. In addition, the Rayleigh number $Ra = GrPr$ will be used in discussing natural convection.

The numerical method is based on a finite-element algorithm previously developed for inert fluid–solid systems. The moving internal boundaries are tracked by an Arbitrary Lagrangian–Eulerian (ALE) technique. Details of the method, including its convergence with mesh refinement, have been discussed previously (Hu et al., 1992; Feng et al., 1994; Hu et al., 2001). Its performance on simulating thermal convection has been validated by Gan et al. (2003). The novel feature here is the evolving melting front. Eq. (13) is implemented explicitly at every time step: the temperature gradient in the fluid at the previous time t_{i-1} determines how thick a solid layer is to be melted by the current time t_i, and the boundary nodes are shifted inward by that thickness along the normal direction. In moving the particle from t_{i-1} to t_i, the mass and moment of inertia at t_{i-1} is used in Eqs. (11) and (12). This is tantamount to assuming that the melt layer sticks on the solid core during the time interval $t_i - t_{i-1}$.

3. Test problems

This section has two objectives: to validate our numerical scheme for melting by solving problems with known solutions, and to understand melting and changes in surface morphology on a fixed particle. The insights gained in these simpler problems will serve as guidelines for the sedimentation simulations in the next section.

3.1. Freezing on a stationary cylinder

There are few experimental or numerical results in the literature for particles melting in a flow. Thus, we have first validated our scheme for deforming the interface Eq. (13) using the freezing on a cylinder in the absence of flow, for which a similarity solution exists (Carslaw and Jaeger, 1960). If the melting temperature is T_m and the subcooled fluid temperature far from the cylinder is T_0, then the radius of the cylinder grows, owing to freezing at Stefan number St, according to:

$$R(t) = 2\lambda\sqrt{\alpha t}, \tag{14}$$

where α is the thermal diffusivity of the fluid and λ is determined by $\lambda^2 e^{\lambda^2} Ei(-\lambda^2) + St = 0$, with Ei being the exponential integral function. The temperature field in the fluid is given by

$$T(r) = T_0 + \frac{T_m - T_0}{Ei(-\lambda^2)} Ei\left(-\frac{r^2}{4\alpha t}\right). \tag{15}$$

While the lack of an intrinsic length scale is a precondition for the similarity solution, our numerical calculation necessarily introduces length scales. Thus, we enclose our particle in a square box and impose initial and boundary conditions derived from the exact solution, the initial time being arbitrarily chosen to be $t = 1$. The subsequent evolution of the solution, as predicted by our numerical scheme, agrees with the analytical solution very well. The growth of the solid radius follows the exact solution to within 0.3% (Fig. 2a), and the temperature profile agrees with the exact solution within 0.7% (Fig. 2b). These results are obtained with 120 nodes on the solid surface, which is the resolution used in the dynamic simulations.

3.2. Melting of a fixed cylinder with natural convection

The next two testing problems involve melting with convection, for which no quantitative comparison as in Fig. 2 can be made. Instead, we will focus on interrogating the numerical results for an understanding of the physical mechanisms which are likely to be at work for settling particles as well.

A solid particle of diameter d is fixed at the center of a rectangular box of height $15d$ and width $4d$. The bottom and the side walls are solid with vanishing velocity and a constant temperature $T_0 = 1$. The top of the box is open, with vanishing stresses and heat-flux. The particle has a constant temperature $T_m = 0$. Other parameters are $Pr = 0.7$, $Ra = 800$ and $St = 2.5125 \times 10^{-2}$. The characteristic velocity of natural convection is $U = \rho_0 \beta \Delta T d^2 g/\mu$, and time is scaled by $\mu/(\rho_0 \beta \Delta T dg)$.

The cold particle induces a downward convection which is further enhanced by the cold melt being produced on the surface. Because of the nonuniform flow and temperature fields, the

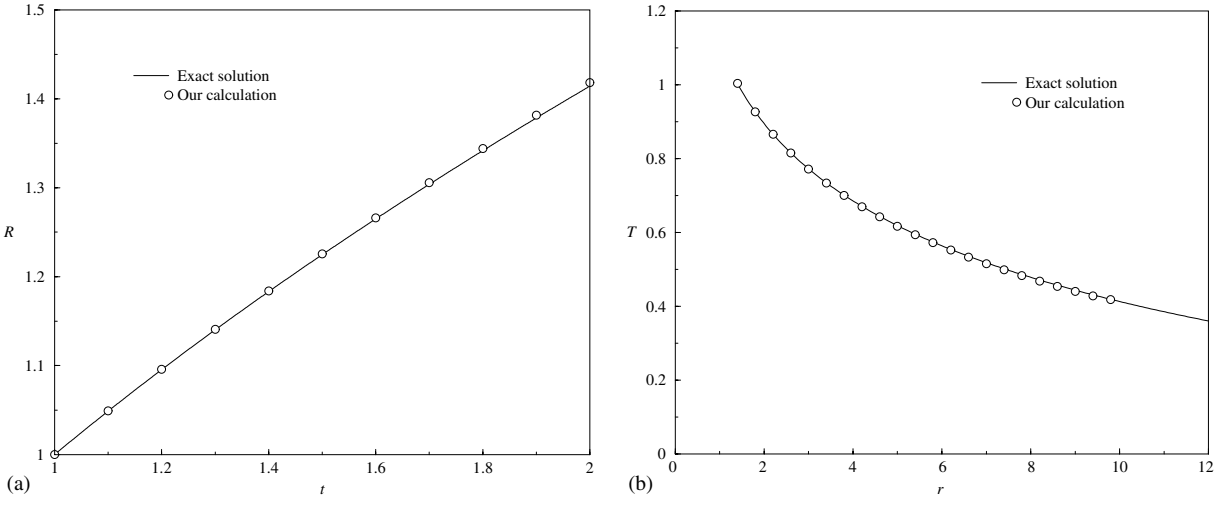

Fig. 2. Validation of our melting scheme for freezing on a cylinder. The parameters are $St = 5.025 \times 10^{-3}$, $\alpha = 328.9$, $\lambda = 2.757 \times 10^{-2}$, $T_0 = 0$ and $T_m = 1$. (a) Growth of the cylinder radius R in time. The time step $\Delta t = 5 \times 10^{-3}$, and the data points are shown every 20 steps for clarity. (b) Temperature profile at $t = 2$, with $R = 1.414$ at this instant.

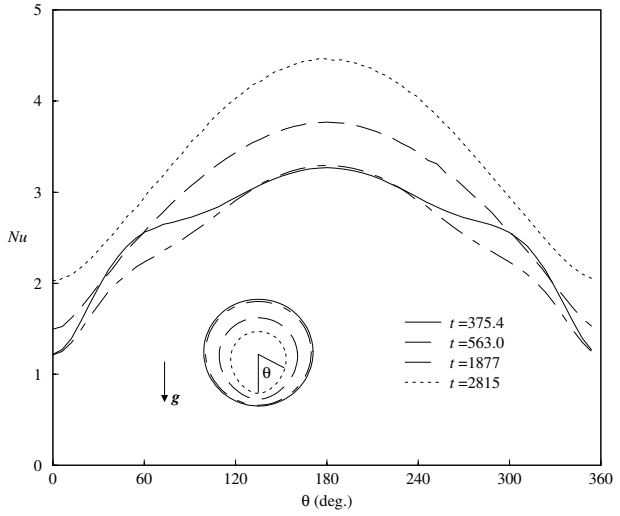

Fig. 3. Evolution of the shape and local heat transfer on a melting cylinder subject to natural convection. *Nu* is defined using the initial diameter of the cylinder, and θ is defined with respect to the initial center of the cylinder.

particle shrinks nonuniformly around its surface, and in time develops a distinctive almond shape, with a round top and a pointed bottom. This shape can be understood from the *Nu* profiles in Fig. 3, which directly determines the local melting rate through Eq. (13). As expected, the heat transfer is maximum at the top of the particle ($\theta = 180°$), where the *Nu* profile is relatively flat. This keeps the top round; the arc may even flatten slightly since the apex melts down a little more than the shoulders. In contrast, *Nu* is minimum at the bottom ($\theta = 0°$). A pointed tip develops because the nadir melts less than the points on either side. A curious feature of the $Nu(\theta)$ profiles is the shoulders around $\theta = 60°$ and 300° shortly after the melting starts ($t = 375.4$). This has been shown to correspond to the maximum shear-rates in those regions as the cold melt sweeps down. As the flow develops, the shoulder shifts downstream and disappears. Since *Nu* is defined using the initial particle diameter, the elevation of the *Nu* curves in time implies that the surface heat flux increases as the particle gets smaller. This is a well-known phenomenon documented by numerous experiments (e.g., Chapman, 1984, Section 9.4).

The only relevant work that we found in the literature is McLeod et al. (1996) who reported an experiment on melting wax spheres in water. The wax is miscible with water but the dissolution is slow so the molten wax flows essentially as a separate fluid phase heavier than water. Despite this difference, the upper part of the particle has a similar shape in the two studies: circular in Fig. 3 and hemispherical in McLeod et al. (1996). On the under side, the wax layer detaches from the sphere and breaks up into ropy strands. This creates an irregular pitted surface which is, of course, absent from our simulation.

3.3. Melting of a fixed cylinder with forced convection

The geometry of the problem is the same as the previous one except that the bottom of the box is also open. A uniform upward flow at $Re = 20$ is imposed at the bottom and the side walls. This

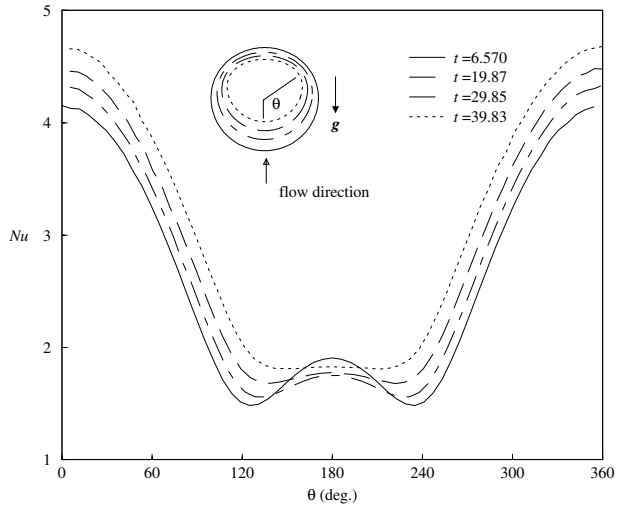

Fig. 4. Evolution of the shape and local heat transfer on a melting cylinder subject to forced convection. The Reynolds number, defined using the uniform inlet velocity U and the initial diameter d, is $Re = 20$. Time is scaled by d/U.

roughly corresponds, after a Galileo transformation, to the settling of a melting particle though in the latter case the particle's velocity relative to undisturbed fluid may not be constant. Natural convection is still retained with $Ra = 800$.

The most notable feature is the shape of the particle. The upstream part (bottom) remains circular and recedes fast because of the high heat flux. The top melts much more slowly, so much so that protruding shoulders form near $\theta = 150°$ and 210°, giving the particle a flattened shape (Fig. 4). This is in contrast to Fig. 3, where the particle is much narrower, and the downstream side is pointed. Again we study the heat transfer around the particle for clues to the evolving shape. During the early times, $Nu(\theta)$ has a local maximum at the back stagnation point ($\theta = 180°$). This is evidently a result of the natural convection drawing hot fluid onto the top of the particle. Thus the apex of the particle melts more than its surrounding areas, flattening the top of the particle. Later, as melting progresses, the local maximum gradually disappears and an essentially constant Nu prevails on the downstream side. This preserves the flatness of the surface. On the front, the high heat transfer rate causes fast melting which produces the oblate shape.

4. Sedimentation of a single particle

We release a particle of initial diameter d, with zero initial velocity, on the centerline of a channel of width W (cf. Fig. 1). The computational domain moves with the particle, its top and bottom being $15d$ and $10d$ from the particle center. Numerical experiments have confirmed that the domain is long enough for the results to be insensitive to the position of the top and bottom. The following parameters are fixed: $Pr = 0.7$, $\rho_s/\rho_0 = 1.00232$, and $W = 4d$. A wider channel ($W = 8d$) has also been used, with qualitatively similar results. The characteristic velocity U is taken to be the maximum settling velocity, and time t is scaled by d/U. Mesh refinement has been

performed to verify convergence of the results and adequate resolution of the thermal and momentum boundary layers. Fig. 5 compares simulations on two meshes for a sedimenting and melting particle. The agreement is very good, and all subsequent simulations use the denser mesh with 120 nodes on the particle surface.

In the absence of thermal effects and melting, the sedimentation of a circular particle in a channel has four *Re*-number regimes (Feng et al., 1994). The parameters used here correspond to the first regime with steady settling along the centerline at $Re = 21.0$. Melting adds three pieces of new physics to the dynamics of a particle: the shrinking size, inertia and weight of the particle, the flow of the newly melted layer down the particle surface, and the downward thermal convection induced in the neighborhood of the particle. The following two limits are clear. At vanishing Stefan number, there is little melting and the behavior of the cold non-melting particle described by Gan et al. (2003) should be recovered. Furthermore, if the particle is heavy and the fall velocity is high, then thermal convection is dominated by forced convection, and the sedimentation reverts to that of an isothermal particle (Feng et al., 1994). For large Stefan numbers, on the other hand, melting is so rapid that no dynamics has time to develop before the particle disappears. In the following, we investigate sedimentation at moderate *Re* and *St* values, for which two *Gr*-regimes can be identified.

Regime A ($0 < Gr < 900$): In this regime, the particle falls along the centerline. The settling velocity $u(t)$, indicated by an instantaneous $Re(t)$ in Fig. 6, rises initially. Apart from gravity, this acceleration is aided by the downward convection of the cold fluid near the particle; the acceleration is larger for higher *Gr*. After u reaches its maximum, it declines monotonically with loss of mass. The deceleration is more pronounced for higher *St*. The simulation is terminated when the

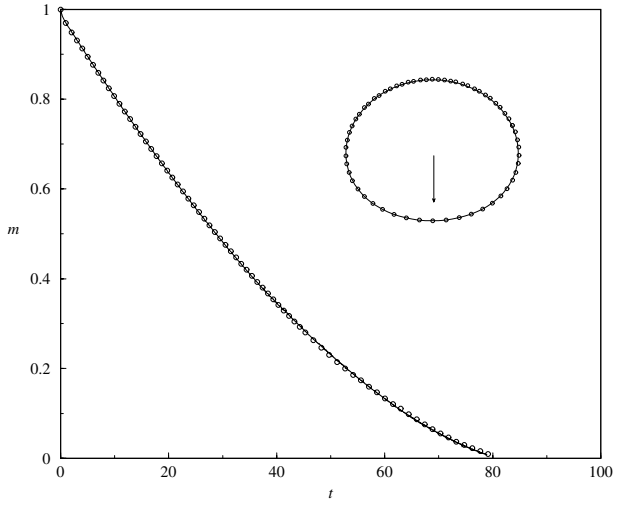

Fig. 5. The decreasing mass of a melting particle computed using two different meshes at $Re = 21.1$, $Gr = 100$ and $St = 2.5125 \times 10^{-2}$: the solid curve has 120 nodes on the particle surface and 4241 total nodes, while the data points, drawn every 20 time steps, have 60 nodes on the particle surface and 3327 total nodes. The inset compares the shape of the particle at $t = 47.64$, the arrow being the direction of fall. The circles indicate the position of the surface nodes for the coarser mesh.

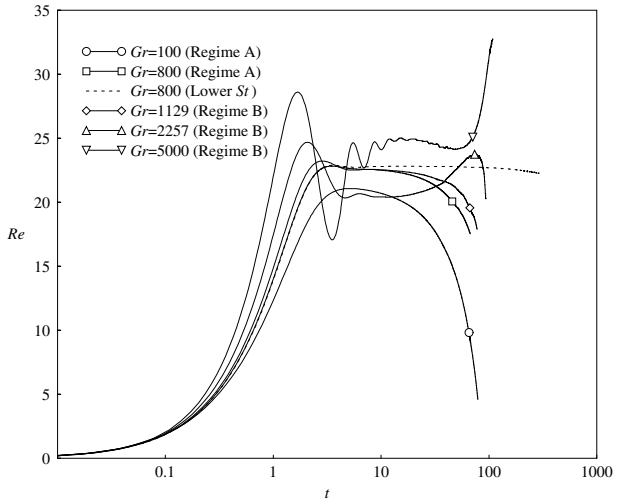

Fig. 6. Sedimenting velocity of a melting particle represented by the instantaneous Reynolds number $Re(t)$. The Stefan number $St = 2.5125 \times 10^{-2}$ except for the dotted curve, for which $St = 1.2563 \times 10^{-3}$.

particle becomes too small to be resolved accurately. This typically occurs after the mass of the particle falls below 5% of its initial value.

Note that for sufficiently high St, a melting particle exhibits the above behavior at any Gr; none of the dynamics described below, including regime B, exists. If St is small enough, on the other hand, another interesting phenomenon sets in. The particle initially falls along the centerline, but gradually develops a small-amplitude laterally oscillation (Fig. 7a). The cause is vortex shedding precipitated by the cold "boundary layer" on the particle. In a reference frame fixed on the particle, the layer of cold melt tends to flow downward and thus counters the upward momentum of the outside fluid. This destabilizes the wake and gives rise to vortex shedding. Similar oscillation has been noted for a settling cold particle without melting (Gan et al., 2003) and for a particle in the absence of any thermal effect (Feng et al., 1994). In the former, vortex shedding is prompted by the downward thermal convection in the particle's wake, provided Gr is high enough. In the latter, vortex shedding occurs "naturally" for Re higher than a threshold value, which is approximately 70 in a channel of $W = 4$. The oscillation eventually dies out for the melting particle when it becomes too small.

Regime B ($Gr > 900$): This regime is characterized by migration of the particle off the centerline toward the channel wall (Fig. 7b). The deviation from the centerline starts gradually, but shows no sign of slowing down till the end of the simulation when the particle becomes too small to track accurately. As soon as the particle deviates from the centerline, it starts to rotate slowly in the normal sense, i.e., as if rolling down the nearby wall (Liu et al., 1993). The rotation never exceeds 60° in all cases. As will be seen shortly, this corresponds to the particle, made oblong by melting, putting its broadside perpendicular to its trajectory.

The lateral migration is an outcome of the conflict between the upward external flow (forced convection), relative to the particle, and the downward natural convection in the wake (Fig. 8a). The latter impinges on the back of the particle and creates a pressure maximum (Fig. 8b). This,

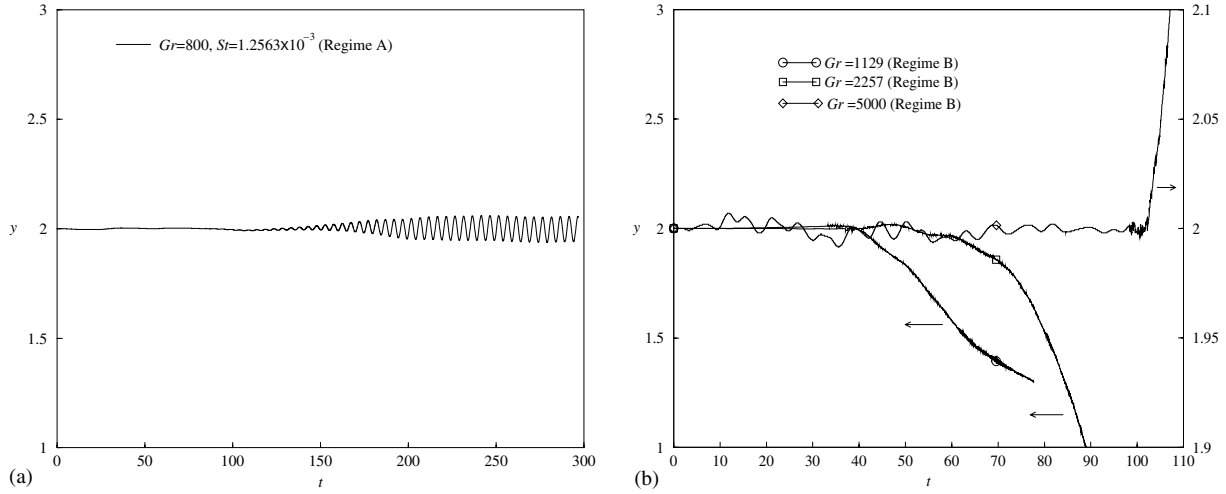

Fig. 7. Lateral position y of a melting particle in a channel of width $W = 4$. (a) Lateral oscillation appears in regime A for small St. For larger St the particle stays on the centerline (not shown). (b) The particle migrates off the centerline in regime B. The curve for $Gr = 5000$ uses the finer scale on the right ordinate. The jitters on the trajectories are a numerical artifact due to the removal of interfacial nodes as the particle shrinks.

along with the high pressure at the front stagnation point, sets up a ''buckling instability''. If some disturbance due to numerical error moves the particle slightly to the left, say, then both the forced and natural convections will tend to go around the right side of the particle. The pressure maxima shift to the right and gives rise to a lateral force that pushes the particle further to the left. Settling along the centerline is thus destabilized. A similar scenario is observed for a non-melting cold particle settling in a hotter fluid (Gan et al., 2003). A notable difference, however, is that for the melting particle, lateral migration prevails for all the higher Gr numbers we tested. For the non-melting particle, on the other hand, the centerline becomes once again a stable position for higher Gr. The re-stabilization is caused by increased wall repulsion at higher Gr as the wake gets wider. This mechanism is absent or at least ineffective for melting particles whose shrinking size implies decreasing wall effect. Thus, lateral migration sets in sooner (for higher St) or later (for lower St). In Fig. 7(b), one may also note the small-amplitude oscillation for $Gr = 5000$ which develops quickly after release and persists till the onset of lateral migration. This is due to a Kelvin–Helmholtz instability in the shear layers in the particle's wake. It has a counterpart in the sedimentation of a non-melting cold particle as well (Gan et al., 2003), though the amplitude is smaller here because of the diminishing size of the particle.

The solutions in regime B exhibit several other features distinctive of melting particles. The first is the oblate shape that the particle develops during sedimentation, with a flat back and a round front. This is the same shape as emerges for a fixed particle melting in a hot stream (cf. Section 3.3), and it appears for lower Gr in regime A as well. Secondly, for higher Gr values, the settling velocity u goes through over- and undershoots initially, but then increases in time despite the loss of mass and proximity of the side wall (Fig. 6). For $Gr = 2257$, u reaches a maximum and then drops as the particle gets very small. For $Gr = 5000$, u continues its rise till the end of the simulation. This curious phenomenon is caused by the flow of the newly melted cold fluid down the

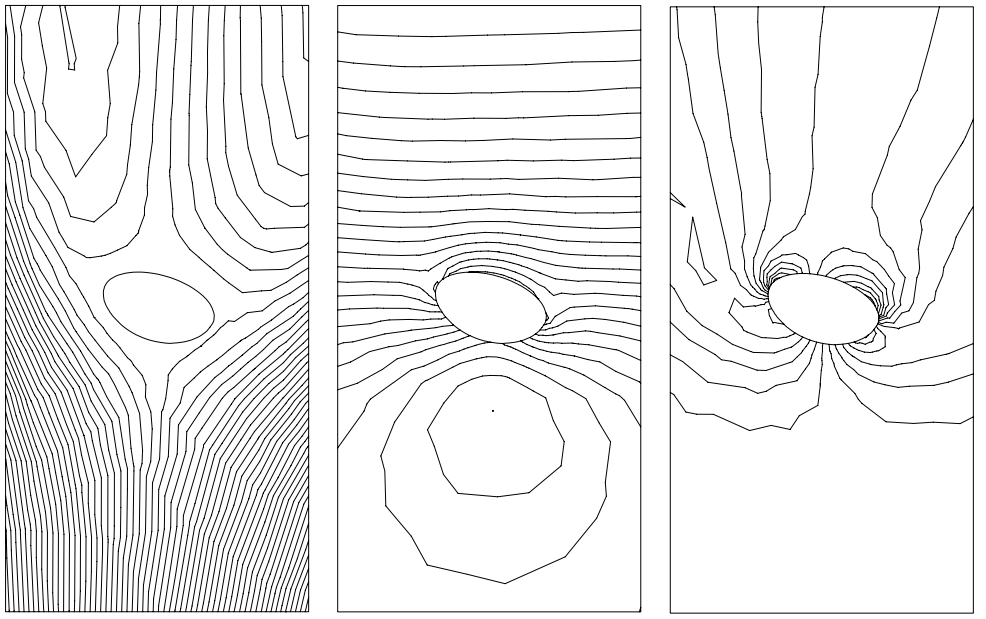

Fig. 8. Magnified view of the local flow field around a melting particle at $t = 81.89$, $Gr = 2257$. The center of the particle is at $y = 1.44$ in a channel of width 4, and the width of the view box is 1 (i.e., the initial particle diameter). (a) Streamlines in a reference frame fixed on the particle's center of mass; (b) pressure contours; (c) vorticity contours, which also reveal the variation of shear stress on the particle surface as the vorticity equals the shear-rate there.

particle. The effects of this mobile melt layer can be inferred from the local flow field in Fig. 8. The density of the streamlines indicates that the downward convection has a lower speed than the upward external flow (Fig. 8a). Yet, the shear stress maxima on top of the two shoulders are much larger than those underneath the particle (Fig. 8c). The former, therefore, is due largely to the shedding of the melt layer. This mechanism enhances the fall velocity of the particle so much that u sometimes increases despite the decreasing gravity force on the particle.

The third notable feature of regime B is the orientation of the particle. It is well known that an oblong particle tends to put its long side perpendicular to the direction of fall (Huang et al., 1994). So our melting particle tilts during lateral migration in such a way that its longer dimension is more or less orthogonal to its trajectory. At the time depicted in Fig. 8, the long axis of the particle is at an angle of 25° with the horizontal. An isothermal ellipsoid released at such an orientation would zigzag because of the high pressure at the front stagnation point (Feng et al., 1994). The melting particle, on the other hand, is driven not only by gravity but also by the downward melt flow. This creates a broad high-pressure region on the back which stabilizes the orientation against swinging (Fig. 8b). The large shear stress on the shoulders (cf. Fig. 8c) may also play a role.

Fig. 9 plots the dwindling mass of the particle for various Gr values. As the particle shrinks, grid points are shifted and sometimes removed from the particle surface. Numerical errors in calculating the particle's mass and moment of inertia generate spurious jitters on the curves, noticeable also in Fig. 7(b). Generally, the melting rate is smaller for higher Gr; this is true even if

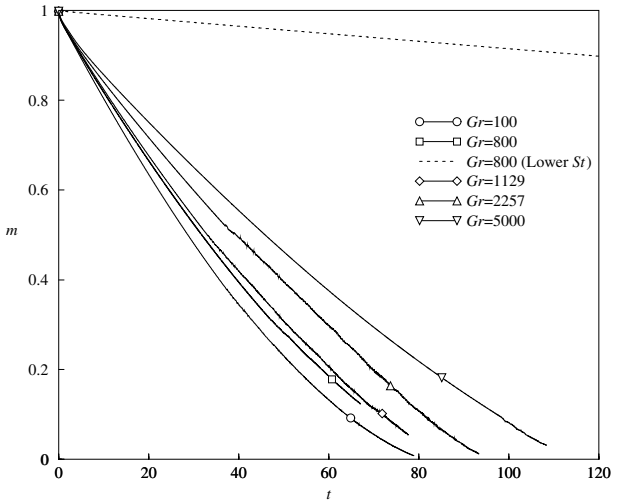

Fig. 9. The diminishing mass of melting particles at various Gr values. The Stefan number $St = 2.5125 \times 10^{-2}$ except for the dotted curve, for which $St = 1.2563 \times 10^{-3}$.

the mass is plotted against the dimensional time. A possible explanation is that at higher Gr, the downward convection covers more of the particle surface with colder fluid, thus hindering heat transfer toward the particle. This seems to be born out by the temperature contours in Fig. 10. Those for $Gr = 100$ feature a cold wake and large temperature gradients in the front (cf. Fig. 4). For $Gr = 5000$, thermal convection pushes the colder fluid forward, lowering the temperature gradient over much of the particle's surface. With slower melting, the larger particle incurs stronger wall repulsion, which delays the onset of lateral migration at higher Gr (Fig. 7b). To sum up Section 4, a melting particle resembles a non-melting cold particle insomuch as its sedimentation is affected by the antagonism between natural and forced convections. But the shrinking size and the flow of the melt layer endow the melting particle with peculiar dynamics during its sedimentation.

5. Sedimentation of doublets

Without thermal effects or melting, the signature behavior of a settling doublet is the drafting-kissing-tumbling (DKT) scenario. This was first observed experimentally (Fortes et al., 1987) and later confirmed by numerical simulations (Hu et al., 1992, 2001). Gan et al. (2003) showed recently that DKT may be completely suppressed by thermal convection if the particle has a different temperature from the fluid. The simulations to be presented here explore additional effects due to melting. As mentioned before, the limiting behavior for very fast or very slow melting is rather uninteresting. We have used moderate values: $St = 5.025 \times 10^{-3}$ and $Re = \mathrm{O}(10)$, and varied Gr from 100 to thousands. The channel width $W = 8d$, and the Prandtl number is fixed at $Pr = 0.7$. The initial configuration of the doublet affects a short transient following release but has no effect on the long-term dynamics. Note that the regimes for a single particle are demarcated by the

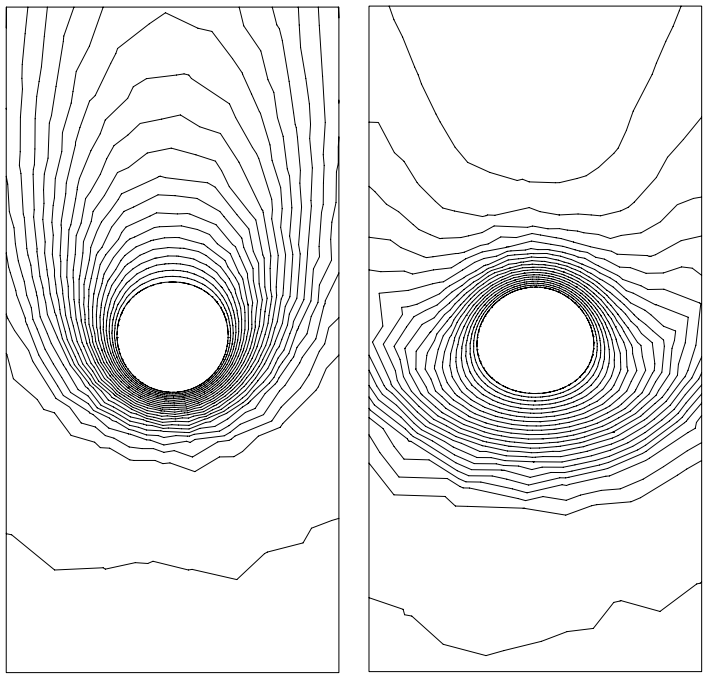

Fig. 10. Temperature contours around a melting particle. (a) $Gr = 100$ at $t = 32.75$; (b) $Gr = 5000$ at $t = 51.70$. In both cases, the mass of the particle is roughly 44% of its initial value.

lateral position y, which depends on wall effects. For doublets, wall effects are largely overshadowed by particle–particle interactions, and lateral migration is no longer a prominent feature.

For smaller Gr, the trailing particle accelerates toward the leading one (''drafting'') and then falls farther behind. This cycle repeats several times without the ''kissing'' and ''tumbling'' phases. Then the two separate vertically to a large distance, which is over $20d$ for $Gr = 100$. The mechanism that suppresses DKT and causes the particles to separate is that the trailer is settling in the cold wake of the leader, and hence encounters more upward buoyancy force. The particles also oscillate laterally because of vortex shedding prompted by the cold melt layer on the particle (cf. Fig. 7a). Not surprisingly, the leader melts faster, and the oscillation eventually dies out as the particles shrink. Except for the shrinkage of the particles, the behavior of a melting doublet at low Gr resembles that of a non-melting cold doublet (Gan et al., 2003).

The dynamics at higher Gr is much more complex, and Fig. 11 depicts a solution at $Gr = 1200$. The sedimentation consists of four stages. Stage I covers the initial period after release ($t < 40$), in which the melting particles behave in essentially the same way as a cold doublet at the same Gr. They go around each other from a distance in a mild form of DKT as discussed in Gan et al. (2003). Entering stage II ($40 < t < 175$), the behavior of cold and melting doublets diverges. At the same Gr, the cold particles tend to separate vertically and the period of DKT lengthens. The melting doublet, on the other hand, gets closer and effectively forms a single long body, which rocks while settling along the center of the channel. This is represented by the synchronized lateral oscillation of the particles in Fig. 11. Note that Fig. 11 shows the y coordinate only, from which

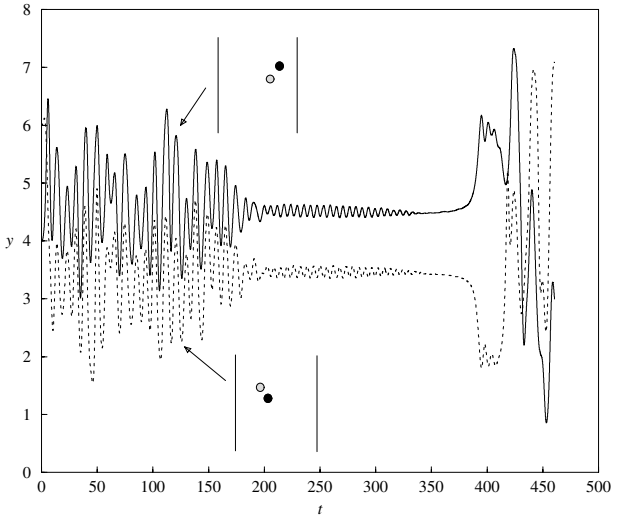

Fig. 11. Lateral positions of a melting doublet at $Gr = 1200$. The insets show the orientation of the doublet when it is closest to the left and right walls. Four stages can be identified, and t is scaled using the initial diameter and the average velocity in stage II ($40 < t < 175$).

stages I and II are not easily distinguishable. The orientation of the line of centers also fluctuates around the horizontal, as shown by the insets. The doublet has a combined wake, which oscillates because of vortex shedding. In all these aspects, the melting doublet behaves as the single elongated body discussed by Feng et al. (1994). The center-to-center distance fluctuates slightly, and both particles rotate as if up the vertical line separating them. The Reynolds number, based on the average settling velocity and the initial diameter, is $Re = 18.8$ in this stage.

Vortex shedding eventually disappears at $t \approx 175$ when each particle has lost roughly half its mass (cf. Fig. 13). This is the beginning of stage III ($175 < t < 375$), in which the doublet settles astride the centerline. The small-amplitude oscillation is due to a Kelvin–Helmholtz instability in the combined wake, similar to the curve for $Gr = 5000$ in Fig. 7(b). Despite the continual loss of mass, the settling speed of the particles increases somewhat as is the case for a single melting particle (cf. Fig. 6).

The pairing behavior in stages II and III forms a remarkable contrast to the repulsion and separation between two isothermal particles (Joseph et al., 1994) or cold non-melting particles (Gan et al., 2003). To investigate the origin of the apparent attraction, we calculated the lateral forces on two cold particles fixed side by side in an upward uniform flow at $Gr = 1200$ and $Re = 18.8$. When the two are close enough, they experience an attraction toward each other, with or without melting. Hence, the mechanism for forming close pairs is present even for non-melting cold particles. However, two cold particles settling side by side is unstable; the particle falling slightly behind will be further ejected upward, either by the buoyancy force in its neighbor's cold wake or by the upward backflow outside the wake. For the solution in Fig. 11, melting enhances the downward thermal convection around the particles. This stabilizes the side-by-side configuration because the high pressure on top of the particles (cf. Fig. 8b) discourages them from separating vertically. Thus, the melting horizontal doublet persists. Fig. 12 shows the velocity,

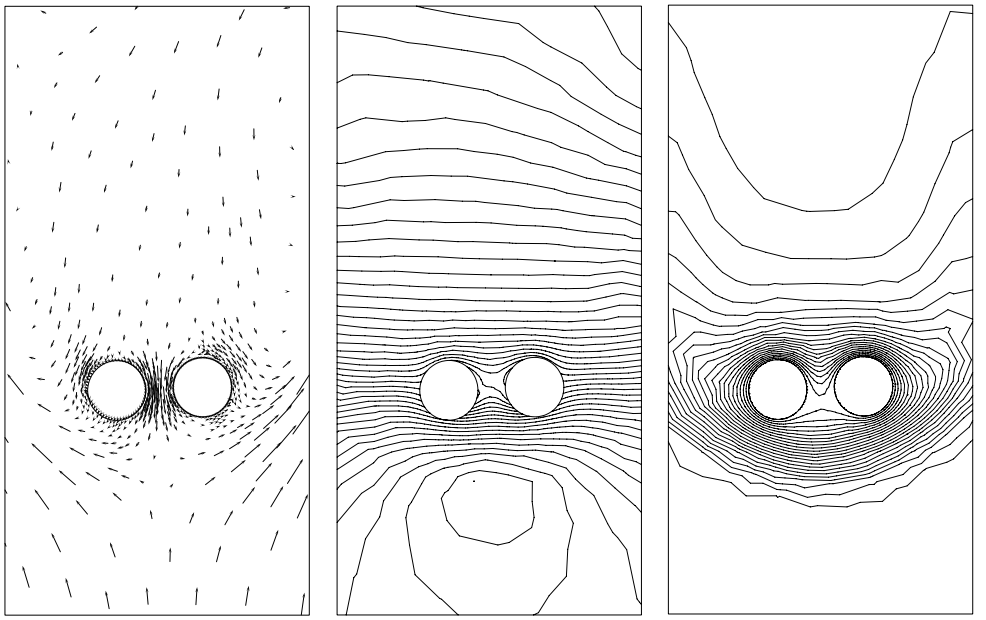

Fig. 12. Magnified views of the velocity field (a), pressure contours (b) and temperature contours (c) around the melting doublet at the beginning of stage III ($t = 181$). The particles are at roughly equal distance from the centerline of the channel, and the width of the view box is 4. The asymmetric pressure distribution on each particle pushes it toward the other.

pressure and temperature fields around the melting doublet at the beginning of stage III ($t = 181$). The downward convection is strong in the gap owing to the low temperature there. Thus, the upward external flow splits ahead of the doublet as if past a single bluff body. The high pressure on the shoulders of the bluff body tends to squeeze the particles together, giving rise to the attraction noted above.

Since the instantaneous Grashof number scales as the diameter cubed, it declines more quickly than the instantaneous Reynolds number as the particles shrink. Sooner or later, the buoyancy force will be overpowered by the inertial force, and the thermal convection by the forced convection. This signals the start of stage IV, at $t \approx 375$, when the particle diameter has shrunk to half of its initial value and the instantaneous parameters are $Re = 10.97$ and $Gr = 193$. Thermal convection and melting can no longer maintain the side-by-side configuration. The particles separate horizontally and then settle into a DKT cycle similar to that for an isothermal doublet (Feng et al., 1994). At the end of the simulation ($t \approx 475$), the particle mass is roughly 10.5% of its initial value.

Fig. 13 shows the diminishing mass and shrinking outline of the particles. The melting rate is essentially identical for the pair, and the particles remain mostly round in contrast to the single melting particle (Fig. 8). This is evidently a result of the continuous rotation of the particles, especially during the period when the two are locked in a horizontal configuration (stage III).

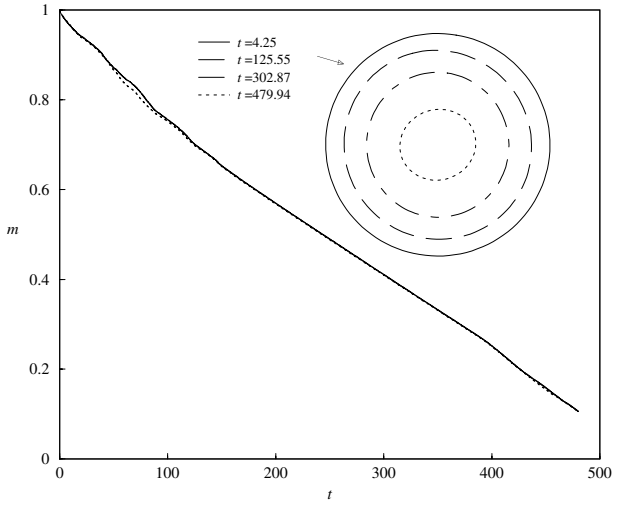

Fig. 13. Evolution of the mass of the melting particles. The shape of the particles is shown at four times representing the four stages.

6. Conclusions

The numerical simulations presented in this paper have born out our assertion that interfacial activities such as melting have profound effects on the interaction of particles. For the moderate *St* and *Re* ranges covered, our results can be summarized as follows. The sedimentation of a single melting particle is dominated by the conflict between the forced and natural convections. Melting changes the surface morphology of the particle, but its direct effect on sedimentation is mostly quantitative. In contrast, the interaction between two particles is qualitatively changed by melting. Drafting-kissing-tumbling is suppressed as a rule. The two particles separate from each other at low *Gr* but attract each other at higher *Gr*. The melt layer helps stabilize the doublet formed by the two particles, which behaves as one elongated body. This behavior, extrapolated to a multi-particle two-phase flow, may lead to aggregation of the particulate phase which would be mostly dispersed in the absence of melting.

Because the simulations are in two dimensions, it would be desirable to test the above speculation with experiments. Unfortunately, we have found little prior work on the motion of particles with interfacial activities. The insights about how melting modifies suspension microstructure should be further investigated in multi-particle simulations and experiments.

Acknowledgements

Acknowledgment is made to the Donors of The Petroleum Research Fund, administered by the American Chemical Society, for partial support of this research. J.J.F. was also supported in part by a 3M Non-tenured Faculty Award and by an NSF Career Award. We thank Professors A. Acrivos, P.S. Ayyaswamy and G. Tryggvason for stimulating discussions, and Professors Shiyi

Chen and Zhen-Su She and the State Key Laboratory for Turbulence Research at Peking University for sponsoring summer visits by J.J.F. and H.H.H., where part of the work was done.

References

Ayyaswamy, P.S., 1999. Combustion dynamics of moving droplets. In: Cheremisinoff, N.P. (Ed.), Encyclopedia of Environmental Control Technology, vol. 1. Gulf Publishing Co., pp. 479–532.

Bellan, J., 1991. Liquid drop behavior in dense and dilute clusters. In: Oran, E.S., Boris, J.P. (Eds.), Numerical Approaches to Combustion Modeling. AIAA. (Chapter 18).

Carslaw, H.S., Jaeger, J.C., 1960. Conduction of Heat in Solids, second ed. Oxford University Press.

Chapman, A.J., 1984. Heat Transfer, fourth ed. Macmillan Publishing Co.

Chiang, C.H., Sirignano, W.A., 1993. Interacting, convecting, vaporizing fuel droplets with variable properties. Int. J. Heat Mass Transfer 36, 875–886.

Crowe, C.T., 1991. Overview of spray modeling. In: Oran, E.S., Boris, J.P. (Eds.), Numerical Approaches to Combustion Modeling. AIAA. (Chapter 17).

Delnoij, E., Kuipers, J.A.M., van Swaaij, W.P.W., 1997. Computational fluid dynamics applied to gas–liquid contactors. Chem. Eng. Sci. 52, 3623–3638.

Feng, J., Hu, H.H., Joseph, D.D., 1994. Direct simulation of initial value problems for the motion of solid bodies in a Newtonian fluid. Part 1. Sedimentation. J. Fluid Mech. 261, 95–134.

Fortes, A.F., Joseph, D.D., Lundgren, T.S., 1987. Nonlinear mechanics of fluidization of beds of spherical particles. J. Fluid Mech. 177, 467–483.

Gan, H., Chang, J., Feng, J.J., Hu, H.H., 2003. Direct numerical simulation of the sedimentation of solid particles with thermal convection. J. Fluid Mech. 481, 385–411.

Hao, Y., Prosperetti, A., 2000. The collapse of vapor bubbles in a spatially non-uniform flow. Int. J. Heat Mass Transfer 43, 3539–3550.

Hu, H.H., Joseph, D.D., Crochet, M.J., 1992. Direct simulation of fluid particle motions. Theoret. Comput. Fluid Dyn. 3, 285–306.

Hu, H.H., Patankar, N.A., Zhu, M.Y., 2001. Direct numerical simulations of fluid–solid systems using the arbitrary Lagrangian–Eulerian technique. J. Comput. Phys. 169, 427–462.

Huang, P.Y., Feng, J., Joseph, D.D., 1994. The turning couples on an elliptic particle settling in a vertical channel. J. Fluid Mech. 271, 1–16.

Ishii, M., 1975. Thermo-Fluid Dynamic Theory of Two-Phase Flow. Eyrolles.

Jackson, C.L., McKenna, G.B., 1990. The melting behavior of organic materials confined in porous media. J. Chem. Phys. 93, 9002–9011.

Joseph, D.D., 1996. Flow induced microstructure in Newtonian and viscoelastic fluids. In: Proc. 5th World Congr. Chem. Eng., San Diego, vol. 6, AIChE, pp. 3–16.

Joseph, D.D., Liu, Y.J., Poletto, M., Feng, J., 1994. Aggregation and dispersion of spheres falling in viscoelastic liquids. J. Non-Newtonian Fluid Mech. 54, 45–86.

Juric, D., Tryggvason, G., 1998. Computations of boiling flows. Int. J. Multiphase Flow 24, 387–410.

Kerr, R.C., 1994. Melting driven by vigorous compositional convection. J. Fluid Mech. 280, 255–295.

Liu, Y.J., Nelson, J., Feng, J., Joseph, D.D., 1993. Anomalous rolling of spheres down an inclined plane. J. Non-Newtonian Fluid Mech. 50, 305–329.

McLeod, P., Riley, D.S., Sparks, R.S.J., 1996. Melting of a sphere in hot fluid. J. Fluid Mech. 327, 393–409.

Shin, S., Juric, D., 2002. Modeling three-dimensional multiphase flow using a level contour reconstruction method for front tracking without connectivity. J. Comput. Phys. 180, 427–470.

Sirignano, W.A., 1993. Formulation of spray combustion equations. In: Chung, T.J. (Ed.), Numerical Modeling in Combustion. Taylor and Francis. (Chapter 9).

Sirignano, W.A., 1999. Fluid Dynamics and Transport of Droplets and Sprays. Cambridge University Press.

White, F.M., 1991. Viscous Fluid Flow, second ed. McGraw-Hill.